Acta Mech 224, 255–268 (2013)
DOI 10.1007/s00707-012-0756-3

S. K. Kourkoulis · Ch. F. Markides · J. A. Hemsley

Frictional stresses at the disc–jaw interface during the standardized execution of the Brazilian disc test

Received: 20 April 2012 / Revised: 20 September 2012 / Published online: 8 November 2012

Abstract An attempt to more accurately describe the boundary conditions of the standardized Brazilian disc test is presented. Specifically addressed is the problem of quantitatively relating the radial pressure with the tangential (frictional) stresses generated at the disc–jaw interface according to a physically acceptable law. A novel approach is proposed based on the notion that friction is directly related to the mismatch between the tangential components of displacement of the disc and jaw along their common interface due to the different deformability of the two materials. The surface displacements in both jaw and disc are determined using the complex potentials method, and the difference between their tangential components along the common contact arc is calculated. This difference in combination with the radial contact pressure tends to generate relative lateral displacements between the disc and jaw that are counterbalanced by frictional forces. The distribution of friction stresses along the contact rim obtained from the present approach fulfils all physical and intuitive imposed conditions. In addition, it is strongly skewed, attaining its maximum value at two-thirds distance from the centre of the contact arc, in good agreement with the earlier results based on a completely different approach.

1 Introduction

The compression of circular discs between either flat or curved metallic jaws (usually referred to as the Brazilian disc test) was proposed simultaneously but independently by Carneiro [1] and Akazawa [2] as a convenient substitute for the direct tension test for concrete specimens. Today, the test is widely used for a much broader class of materials.

Despite its widespread use, some doubts about its validity are still expressed. The most critical ones are perhaps those related to the influence of the tangential (frictional) stresses developed within the disc–jaw contact area, and (closely connected with these frictional stresses) the premature fractures sometimes appearing in the immediate vicinity of the disc–platen interface.

In [3], Fairhurst attempted a quantification of the influence of these stresses and concluded that "*... care must be taken to minimize tangential stresses along the loaded rim, since these may significantly modify the stresses induced in the disc, making any analysis based on radial loading ... invalid*". Along similar lines,

S. K. Kourkoulis (✉) · C. F. Markides
Laboratory for Testing and Materials, Department of Mechanics, School of Applied Mathematical and Physical Sciences, National Technical University of Athens, 5 Heroes of Polytechnion Avenue, Theocaris Bld., Zografou Campus, 157 73, Athens, Greece
E-mail: stakkour@central.ntua.gr
Tel.:+30-21-07721263
Fax:+30-21-07721302

J. A. Hemsley
Christchurch, Dorset, UK

Colback [4] criticized the use of soft plastics as inserts (load distributors) between the disc and jaw since they "*... are liable to extrude under load and thereby induce tangential tensile stresses ...*". A few years later, Hooper [5] considered the failure mechanisms activated during diametral compression of glass cylinders and emphasized that "*... The mode of fracture ... can be explained at least qualitatively in terms of the tensile stresses generated in the contact region*".

The first attempt to determine analytically the influence of interfacial frictional stresses on the stress field developed in the Brazilian disc is perhaps by Addinall and Hackett [6]. Almost four decades later, Lavrov and Vervoort [7] proposed an analytical solution for a general distribution of tangential traction along the disc–jaw contact rim and obtained the Cartesian components of the stress field in the form of infinite series. Based on the results of their solution, Lavrov and Vervoort concluded that "*... the influence of the friction (shear) force applied over two opposite arcs, on the stress distribution over the major part of the main diameter in Brazilian tests can be neglected in most cases, at least if the magnitude of the tangential stress is <50 % of the radial load*". In addition, it was pointed out that "*...when the magnitude of the tangential stress is of the order of 0.5 of the radial stress, significant changes in the stress field in the vicinity of the boundary are observed ...*" and also that under certain conditions "*... friction can provide even more ambiguity in the interpretation of the test results than it is usually believed*".

It could be argued at this point that tangential stresses equal to 50 % of the respective radial stresses are unlikely to appear in practical applications and that even if this were to be the case, the alteration of the overall stress field is confined to a very small area around the disc–jaw interface. Unfortunately, even this strongly localized alteration could have a crucial influence on the validity of results obtained from Brazilian disc tests. Indeed, using the boundary element method, Lanaro et al. [8] reached the conclusion that "*The boundary conditions ... drastically affect the strength of the simulated Brazilian test results. Negative and positive friction seems to have the same effect on the strength whereas the model with no boundary friction exhibited a much higher strength ...*". Similar conclusions were drawn by Hudson et al. [9] who stressed that "*... cracks initiated directly below the loading points in the Brazilian test for both flat steel platen loading and 10^o radiused end-cap loading for marble and granite specimens. Since failure did not originate at the centre of the disc in the assumed region of maximum tensile stress, the tensile strength value indicated by the Brazilian test is erroneous*".

It therefore becomes clear that before using the results for tensile strength as they are obtained from standardized Brazilian tests, it is imperative to correctly assess the influence of the tangential stresses. The main limitation of existing studies is that the distribution of frictional stresses adopted is more or less arbitrary, for example, either sinusoidal [6,7] or uniform with a discontinuity at the axis of symmetry [10]. In addition, there is no attempt to correlate quantitatively the frictional stresses with the externally applied radial pressure. Perhaps, the reason for this is that a direct connection based on Coulomb's law (dry friction) is inappropriate and leads to results unacceptable from the physical point of view. Indeed, a mechanistic application of Coulomb's law leads to maximization of friction forces at the centre of the contact arc where it is clear by intuition that, due to symmetry, friction must be zeroed.

The basis of the present work is that friction must somehow be related not only to the nature of the materials and the externally applied radial pressure, but also to the mismatch of the tangential displacements of adjacent points on the disc and the jaw that come into contact. Accordingly, the Brazilian disc problem is revisited herein as a simplified contact problem, the solution of which yields the displacement mismatch that in turn is used to obtain closed-form expressions for the frictional stresses developed at the disc–jaw interface. The resulting distribution of frictional stresses is in good qualitative agreement with those obtained earlier, both theoretically and experimentally [5,11,12], as will be discussed in the following sections. Finally, a brief parametric analysis is undertaken to reveal some interesting points concerning the crucial factors influencing the distribution of frictional stresses.

2 Physical considerations and theoretical assumptions

2.1 The problem

Consider the basic device proposed by the International Society for Rock Mechanics (ISRM) for the standardized Brazilian disc test [13], schematically shown in Fig. 1a. The device consists of two stiff metallic jaws, the interior surface of each having the form of a circular cylinder of radius R_2 equal to $1.5R_1$, where R_1 is the radius of the disc-shaped test specimen. Clearly, before any load is exerted on the upper surface of the upper jaw (and ignoring the self-weight of the jaws), the contact between the disc and the jaw is realized along

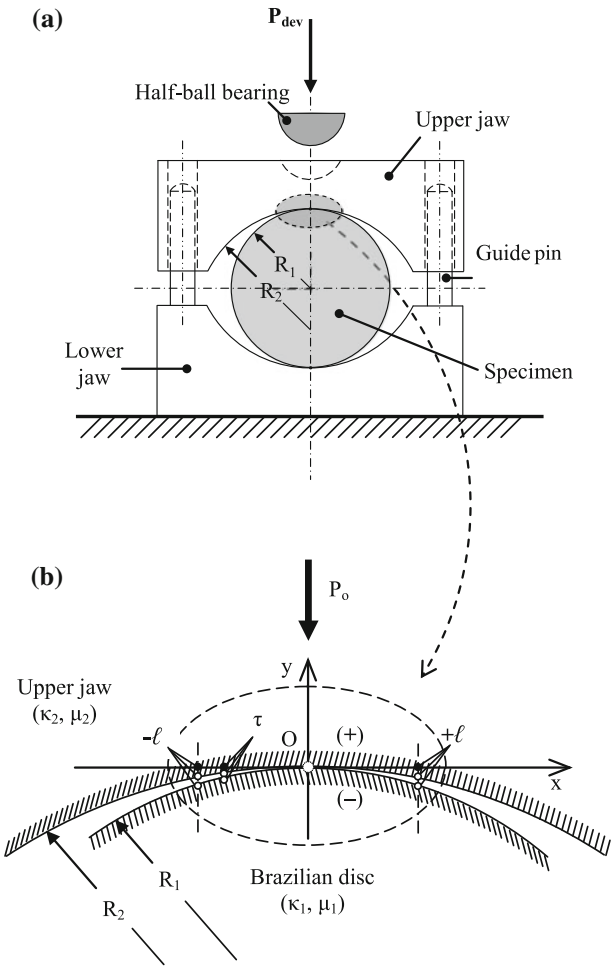

Fig. 1 Standardized Brazilian disc test. **a** Schematic representation of ISRM-suggested device. **b** Definition of symbols used in analysis

a mathematical line (i.e. the common generatrix of the cylindrical surfaces of the disc and the jaw). As the external load P_{dev} increases, it is assumed that contact is realized on a cylindrical surface, the projection of which on the xOy plane is a finite circular arc (symmetric with respect to the central point O) of length 2ℓ which increases with increasing load, and which is usually considered to be very "small" relative to the disc size.

This configuration corresponds to a contact problem of two elastic bodies, where both materials are assumed to be homogeneous, isotropic and linearly elastic. For symmetry reasons only the contact between the disc and the upper jaw is considered herein, and initially such contact is assumed to be frictionless. The solution to the familiar Hertz contact problem is based on Muskhelishvili's complex potentials method [14] in classical plane elasticity. The specific configuration represents a mixed fundamental problem, given that conditions for the displacements as well as for the resultant force are imposed at the contact surface, while outside this region the stresses are zero. The solution gives the length of the contact arc and also the radial contact stresses developed between the disc and the jaws [15]. The main aim of the present analysis is to determine the displacement field developed in both the disc and the jaw.

2.2 Displacement field for the disc and the jaw

The complex potentials of this contact problem were recently derived in closed form by Markides and Kourkoulis [15] following Muskhelishvili's [14] general formulation. The solution was obtained assuming that the contact length 2ℓ is very small compared to the dimensions of both the disc and the jaw, which in turn

are considered as occupying the lower and upper half complex planes, respectively (Fig. 1b). The origin of the Cartesian reference system is taken at the centre of the contact arc. The arbitrary point $z = re^{i\theta}$ of the plane is denoted by τ on the real axis. The potential functions are the following:

$$\Phi_1(z) = \frac{1}{6R_1K}\left(\sqrt{\ell^2 - z^2} + iz\right), \quad \Phi_2(z) = -\Phi_1(z), \tag{1}$$

where

$$K = \frac{\kappa_1 + 1}{4\mu_1} + \frac{\kappa_2 + 1}{4\mu_2}. \tag{2}$$

In the above equations the subscripts 1 and 2 relate to the disc and the jaw, respectively. In addition, κ_j, μ_j, $j = 1, 2$, are Muskhelishvili's constants and the shear moduli, respectively, for the disc and jaw materials.

According to this solution [15], the contact length is given as

$$2\ell = 2\sqrt{\frac{6R_1KP_o}{\pi}} \tag{3}$$

with $P_o = P_{\text{dev}}/w$ (Fig. 1b), where w is the disc thickness. Integrating Eqs. (1) gives

$$\left.\begin{matrix}\varphi_1(z)\\ \varphi_2(z)\end{matrix}\right\} = \pm\frac{1}{12R_1K}\left(z\sqrt{\ell^2 - z^2} + \ell^2 \text{Arc tan}\frac{z}{\sqrt{\ell^2 - z^2}} + iz^2\right) + \left\{\begin{matrix}C_1\\ C_2\end{matrix}\right. \tag{4}$$

where C_1, C_2 are in the general case complex constants related to rigid body displacements. As a next step, Eq. (4) is substituted in Muskhelishvili's [14] well-known expression for the displacements, namely

$$2\mu_{1,2}(u_{1,2} + iv_{1,2}) = \kappa_{1,2}\varphi_{1,2}(z) + \varphi_{1,2}(\overline{z}) - (z - \overline{z})\overline{\varphi'_{1,2}}(\overline{z}). \tag{5}$$

Then letting z tend to $\tau \in [-\ell, +\ell]$ from the lower $(-)$ and upper $(+)$ half planes, respectively, and further assuming that the rigid body displacements are zero (so that the point $z = 0$ remains fixed), the horizontal (tangential) u_j and vertical (radial) v_j, $j = 1, 2$, components of the displacement field for any point on the disc $(j = 1)$ and the jaw $(j = 2)$ along their common contact arc are obtained in closed form as:

$$u_1^-(\tau) = -\frac{\kappa_1 - 1}{24R_1\mu_1K}\left(\tau\sqrt{\ell^2 - \tau^2} + \ell^2 \text{Arc sin}\frac{\tau}{\ell}\right), \qquad v_1^-(\tau) = \frac{\kappa_1 + 1}{24R_1\mu_1K}\tau^2, \tag{6}$$

$$u_2^+(\tau) = -\frac{\kappa_2 - 1}{24R_1\mu_2K}\left(\tau\sqrt{\ell^2 - \tau^2} + \ell^2 \text{Arc sin}\frac{\tau}{\ell}\right), \qquad v_2^+(\tau) = -\frac{\kappa_2 + 1}{24R_1\mu_2K}\tau^2, \tag{7}$$

while noting that these results are also obtained from elementary considerations of the local stress field.

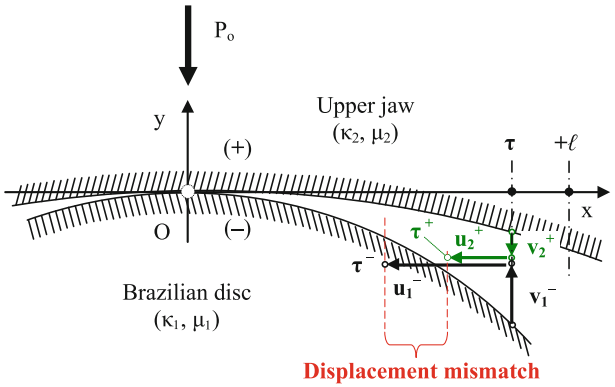

Fig. 2 Schematic representation of displacement mismatch in standardized Brazilian disc test (not to scale)

In the above equations, $u_1^-(\tau)$ and $u_2^+(\tau)$, that is, the horizontal (tangential) displacements at points τ of the disc and jaw, respectively, are both negative on $\tau > 0$. Thus, any two points τ of the disc and the jaw in the contact region, initially facing each other, tend always to move inwards with respect to the Cartesian reference origin. Concerning $v_1^-(\tau)$ and $v_2^+(\tau)$, namely the vertical (radial) displacement components of the disc and the jaw, respectively, it is seen from Eqs. (6) and (7) that the point τ on the disc moves upwards (positive) while the opposite point τ on the jaw moves downwards, in order for the two facing points to come in contact (assuming that rigid body displacements are zero).

3 Frictional stresses along the disc–jaw contact rim

3.1 Displacement mismatch between the disc and the jaw

It is clear from Eqs. (6) and (7) that when the jaws are stiffer than the specimen, as usually happens in practice, it holds that $|u_1^-(\tau)| > |u_2^+(\tau)|$, that is, in the contact region, the local contraction of the disc is greater than that of the jaw. Hence, any two points $\tau \in [-\ell, +\ell]$ of the disc and the jaw initially (before deformation) facing each other tend to shift laterally during loading to points τ^- and τ^+, respectively; in other words, they tend to slide relative to each other. It follows that where the disc and the jaws are made from materials of different deformability, a displacement mismatch inevitably occurs leading to a relative motion tendency. This inward displacement is maximized at the points $\tau = \pm\ell$ and vanishes at $\tau = 0$. A schematic representation of this mechanism is shown in Fig. 2 (not to scale for clarity).

Under frictionless conditions, the horizontal displacement mismatch $U(\tau)$ of any two initially adjacent points τ on the disc and the jaw in the contact region is readily obtained from Eqs. (6) and (7) as

$$U(\tau) = \left|u_1^-(\tau)\right| - \left|u_2^+(\tau)\right| = \frac{1}{24R_1K}\left(\frac{\kappa_1 - 1}{\mu_1} - \frac{\kappa_2 - 1}{\mu_2}\right)\left|\tau\sqrt{\ell^2 - \tau^2} + \ell^2 \mathrm{Arc\,sin}\,\frac{\tau}{\ell}\right|. \tag{8}$$

Obviously, $U(\tau)$ is a real positive number, vanishing at $\tau = 0$ and attaining its maximum value at $\tau = \pm\ell$. This maximum value is

$$U(\tau)_{\max} = U(\ell) = \left|u_1^-(\ell)\right| - \left|u_2^+(\ell)\right| = \frac{1}{24R_1K}\left(\frac{\kappa_1 - 1}{\mu_1} - \frac{\kappa_2 - 1}{\mu_2}\right)\ell^2\frac{\pi}{2}. \tag{9}$$

To obtain a quantitative view of the displacement mismatch, consider a disc of radius $R_1 = 0.05$ m made from Dionysos marble ($E_1 = 80$ GPa, $\nu_1 = 0.25$, $\mu_1 = 32$ GPa) and jaws made from steel ($E_2 = 210$ GPa, $\nu_2 = 0.30$, $\mu_2 = 80.8$ GPa). Then assuming plane strain conditions ($\kappa = 3 - 4\nu$), the elastic constants are $\kappa_1 = 2$, $\kappa_2 = 1.8$, and the elastic parameter from Eq. (2) is $K = 0.032 \times 10^{-8}\,\mathrm{GPa}^{-1}$. Hence, for an external load equal to 12 kN (a force generating a tensile stress at the disc centre close to the average fracture stress of Dionysos marble [16]), the length of the semi-contact arc from Eq. (3) is $\ell = 1.92$ mm, and the variation of $U(\tau)$ from Eq. (8) is plotted in Fig. 3 (secondary y axis).

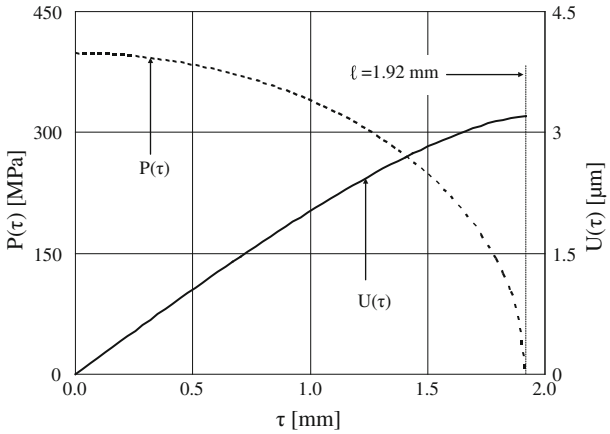

Fig. 3 Variation of radial pressure $P(\tau)$ (primary y axis) and displacement mismatch $U(\tau)$ (secondary y axis) along semi-contact arc for Dionysos marble disc compressed between curved steel jaws ($P_{\text{dev}} = 12\,\text{kN}$)

3.2 Distribution of frictional stresses along the contact rim

3.2.1 Complete stick conditions

Depending on the actual interface conditions, the above displacement mismatch will result in either free relative motion of the disc with respect to the jaw (where the disc and jaw are perfectly smooth) or to the development of tangential (friction) forces along the disc–jaw interface (where the coefficient of friction between disc and jaw is finite). Given that the first case is unlikely to appear in practical applications, attention is focused on the second case.

Although the relation between frictional forces and the displacement mismatch is initially unknown, it could be assumed (at least as a first step) that the radial pressure $P(\tau)$ (developed at the disc–jaw interface due to the compression of the jaw on the disc) and the displacement mismatch $U(\tau)$ are directly proportional to the tangential stresses $T(\tau)$ according to a simple linear relationship. Thus, at an arbitrary point $\tau > 0$ on the contact region, the law here proposed for the frictional stresses is expressed as

$$T(\tau) = f \cdot U(\tau) \cdot P(\tau), \tag{10}$$

where f is a real positive constant (units m^{-1}) depending on the nature of the materials in contact. The proposed method for its experimental determination is discussed later.

The variation of $P(\tau)$ takes the classical semi-elliptical form

$$P(\tau) = \frac{1}{3R_1\text{K}}\sqrt{\ell^2 - \tau^2} \tag{11}$$

and is shown schematically in Fig. 4. For the case of a disc made from Dionysos marble, jaws made from steel, and geometrical and loading conditions identical to those of Sect. 3.1, the variation of $P(\tau)$ along the contact arc is plotted in Fig. 3 (primary y axis) together with the corresponding distribution of $U(\tau)$.

Combining Eq. (10) with Eqs. (8) and (11) gives the frictional contact stresses according to the present approach as

$$T(\tau) = f\frac{1}{72R_1^2K^2}\left(\frac{\kappa_1 - 1}{\mu_1} - \frac{\kappa_2 - 1}{\mu_2}\right)\left[\tau(\ell^2 - \tau^2) + \ell^2\sqrt{\ell^2 - \tau^2}\,\text{Arc sin}\,\frac{\tau}{\ell}\right]. \tag{12}$$

The distribution of frictional stresses along one-half of the contact length is plotted in Fig. 5, again for the case of a Dionysos marble disc and steel jaws, with $P_{\text{dev}} = 12\,\text{kN}$ and various values of the constant f. Also plotted is the distribution of radial pressure developed along the disc–jaw interface, given by Eq. (11).

It is interesting to observe from Fig. 5 that the distribution of $T(\tau)$ over the contact half-width is neither similar to that for the radial pressure nor symmetric with respect to any axis. Moreover, it is not represented by a cosine- or sine-law, as is sometimes assumed in the literature [6,7]. The skewed distribution is zero at the central (loading) axis and at the contact edge, and its maximum value occurs at two-thirds of the contact

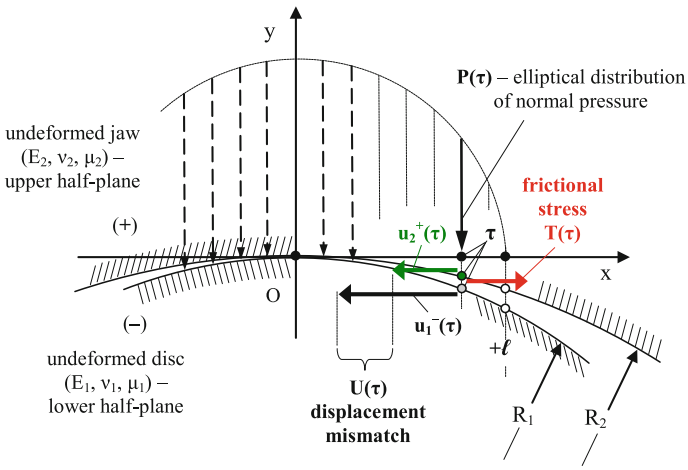

Fig. 4 Mathematical modelling of contact region. The elliptic distribution of normal pressure $P\tau$ and the notion of frictional stress $T\tau$ are also shown.

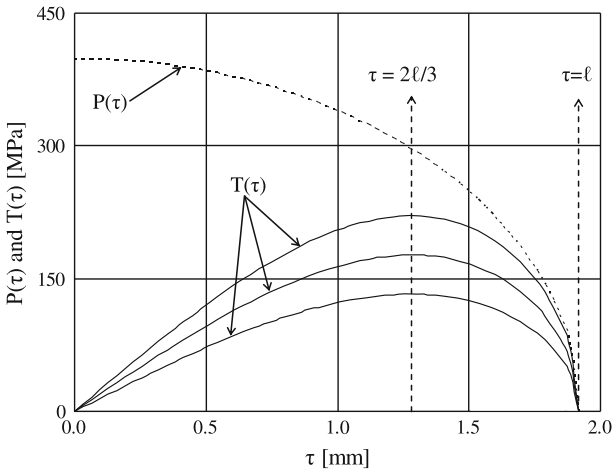

Fig. 5 Radial and tangential contact stresses along semi-contact arc for case of Dionysos marble disc and steel jaws ($P_{\text{dev}} = 12$ kN) for various values of the constant f

length from the centre. Similar skewed distributions of tangential stress obtained by other forms of analysis were reported by Conway and Engel [11] and Hooper [5], while Ghobrial [12] studied the contact stresses developed in rolls during flat rolling using photoelasticity.

3.2.2 Partial slip conditions

In the above discussion it was assumed that the coefficient of friction is of a magnitude prohibiting completely the relative displacement between facing points on the disc and jaw along the contact rim. It could be argued of course that under specific conditions the frictional resistance cannot prevent sliding, at least along part of the contact rim. This mechanism is assumed to be governed by the Amontons–Coulomb law of dry friction according to which the *limiting* friction stress $T_{\max\,\mathrm{A-C}}$, that can be sustained by two bodies in contact is given by the following equation:

$$T(\tau)_{\max\,\mathrm{A-C}} = nP(\tau) = \frac{n}{3R_1K}\sqrt{\ell^2 - \tau^2} \tag{13}$$

in the present case, where n is the coefficient of static friction. The direct relationship between the normalized values of $T(\tau)_{\max\mathrm{A-C}}$ and $P(\tau)$ along the contact rim is plotted schematically in Fig. 6. It is emphasized that $\mathrm{T}(\tau)_{\max\,\mathrm{A-C}}$ represents the limiting (maximum) value of the tangential stress that can be developed along the

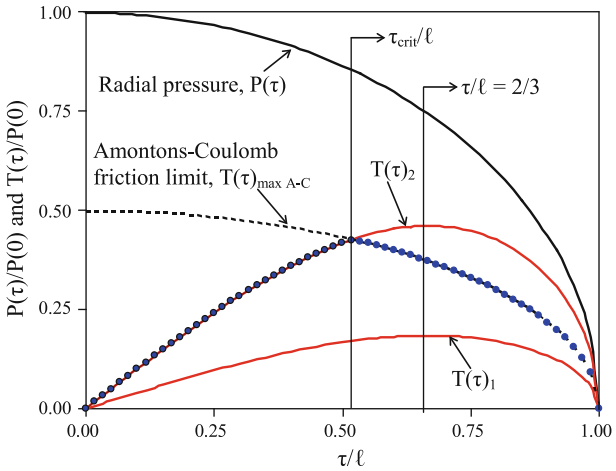

Fig. 6 Normalized variations of radial pressure and frictional stress along semi-contact arc and their relation with Amontons–Coulomb limiting value of static friction

interface of two bodies in contact, and not the actual friction stress $T(\tau)$ that is developed at any moment for an arbitrary value of the force tending to cause relative motion. The latter is given by Eq. (12) as long as

$$T(\tau) < T(\tau)_{\max\ A-C} \tag{14}$$

and is represented in Fig. 6 by the $T(\tau)_1$ curve.

If the condition expressed by Eq. (14) is not satisfied, then inevitably slip will occur along part of the contact length, in fact along the continuous part of the $T(\tau)_2$ curve in Fig. 6. Along this part of the contact length, the friction stress is equal to $T(\tau)_{\max A-C}$, while in the remaining part (the dotted portion of the $T(\tau)_2$ curve), it is still given by Eq. (12). Hence, in the presence of partial slip, the interfacial (frictional) contact stresses are given by:

$$T(\tau) = \begin{cases} f\frac{1}{72R_1^2K^2}\left(\frac{\kappa_1-1}{\mu_1}-\frac{\kappa_2-1}{\mu_2}\right)\left[\tau(\ell^2-\tau^2)+\ell^2\sqrt{\ell^2-\tau^2}\,\mathrm{Arc\,sin}\,\frac{\tau}{\ell}\right], & 0\le\tau<\tau_{\mathrm{crit}} \\ \frac{n}{3R_1K}\sqrt{\ell^2-\tau^2}, & \tau_{\mathrm{crit}}\le\tau\le\tau_{\max} \end{cases} \tag{15}$$

where τ_{crit} denotes the intersection of the $T(\tau)=nP(\tau)$ and the $T(\tau)=fU(\tau)P(\tau)$ curves (Fig. 6).

It is the continuity of the interfacial stresses at the point $\tau=\tau_{\mathrm{crit}}$ on the contact rim that could permit determination of the constant f in Eq. (10). Indeed, at the border of the two regions on the contact rim in cases where the condition of Eq. (14) is not satisfied, it holds that $T(\tau_{\mathrm{crit}})_{\max A-C}=T(\tau_{\mathrm{crit}})$, which is equivalent to the expression

$$f=\frac{n}{U(\tau_{\mathrm{crit}})} \tag{16}$$

In other words if τ_{crit} is determined (either experimentally or numerically), then f can be obtained from Eq. (16) since both n and $U(\tau_{\mathrm{crit}})$ are known.

4 Parametric analysis for complete stick conditions

In this section a short parametric analysis is carried out to establish the dependence of the frictional stresses and related quantities (contact length, maximum displacement mismatch and maximum radial pressure) on some critical parameters, including the relative deformability of the disc and jaw materials, the level of the externally applied load and the geometry. These results could prove helpful both for engineers using the Brazilian test for practical purposes and for researchers dealing with various other aspects of the problem.

In all calculations, the jaws are assumed to be made from steel. Concerning the disc, a broad class of materials is considered ranging from steel to shellstone (a rather soft porous stone used by ancient Greeks for the erection of the Zeus Temple at Olympia) whose modulus of elasticity varies from 1 to 3 GPa [17],

Table 1 Materials considered in the parametric analysis [19]

Material	E (GPa)	ν_{actual}	$\nu_{average}$(*)
Magnesium alloys	**41–45**	0.35	
Aluminium alloys	**70–79**	0.33	
Brass	**96–110**	0.34	**0.34**
Bronze	**96–120**	0.34	
Copper and alloys	**110–120**	0.33–0.36	
Titanium alloys	**100–120**	0.33	
Cast iron A	**83–170**	0.20–0.30	
Monel	**170**	0.32	
Steel A	**190–210**	0.27–0.30	**0.28**
Steel B	**200**	0.28	
Steel C	**210**	0.30	
Nickel	**210**	0.31	
Shellstone	**2–3**	0.25	
Sandstone	**50**	0.20–0.30	**0.25**
Granite A	**40–100**	0.20–0.30	
Concrete	**17–31**	0.10–0.20	**0.19**
Glass	**48–83**	0.17–0.23	

* Values used in parametric analysis

thereby covering almost the whole range of materials that could be tested using the ISRM device. For practical reasons, emphasis is given to the very brittle Dionysos marble (extensively used in the restoration project of the Acropolis of Athens monuments) and to the relatively more ductile Poly-methyl-meth-acrylate (commercially known as PMMA) which is an easily shaped material and therefore suitable for thorough experimental studies. Concerning the numerical values of the constant f, advantage was taken of the results of a recent numerical study of the problem [18], according to which, in cases where the condition of Eq. (14) is not satisfied, the part of the contact length along which stick conditions prevail is equal to about 25 % of the contact half-length.

4.1 Influence of the relative deformability

The relative deformability of the disc and jaw materials is perhaps the most important parameter since it dictates both the extent of the contact length and the magnitude of the displacement mismatch. For practical reasons, and given that Poisson's ratio also influences the results, the materials here considered are grouped into four classes, as indicated in Table 1 [19], with an average value of Poisson's ratio assigned to each group.

In Fig. 7a, the extent of the semi-contact arc is plotted versus the relative deformability of the disc and jaw materials, expressed in terms of the ratio of their moduli of elasticity, for example, the $E_{\text{disc}}/E_{\text{jaw}}$ ratio. A common external load equal to 12 kN is again assumed to be exerted for all materials. Such an assumption is acceptable since the solution is based on the linear elasticity assumption and therefore no attention is paid to the fracture stress of the materials. The embedded figure corresponds to materials with a very low modulus of elasticity (e.g. shellstone). The behaviour of all four material classes is described by more or less the same curve despite the differences in their Poisson's ratio, and the contact arc ranges from about 1.5° for $E_{\text{disc}}/E_{\text{jaw}} \to 1$ (very stiff specimens) to about 12° for $E_{\text{disc}}/E_{\text{jaw}} \approx 0.01$ (very soft porous stones like the shellstone). However, since the analysis described in Ref. [15] is based on the small contact arc assumption, the results for $E_{\text{disc}}/E_{\text{jaw}} \to 0$ must be considered with some caution regarding their accuracy.

Results showing the dependence of the maximum relative horizontal displacement on the relative deformability are plotted in Fig. 7b, again for all four classes of material. It is now seen that the role of Poisson's ratio is much more evident. If $E_{\text{disc}}/E_{\text{jaw}} = 0.25$, for example, the relative displacement when $\nu = 0.25$ is more than five times greater than that for materials with $\nu = 0.19$ and the same relative deformability. For the two classes of particular interest to the engineering community (i.e. those for $\nu = 0.19$ and $\nu = 0.25$, encompassing concrete and most natural building stone), the displacement mismatch varies from about 1 μm to 5 μm. For values of the $E_{\text{disc}}/E_{\text{jaw}}$ ratio approaching unity, the relative displacement disappears, and there are no friction forces even for nonsmooth surfaces. For shellstone, which is not included in Fig. 7b, the displacement mismatch is about 16 μm.

Finally, the dependence of both the maximum radial pressure and maximum frictional stress (i.e. $P_{\max} = P(0)$ and $T_{\max} = T(2\ell/3)$) on the $E_{\text{disc}}/E_{\text{jaw}}$ ratio is plotted in Fig. 8, again for the four classes of material. It is seen that both quantities are rather insensitive to the value of Poisson's ratio. It is emphasized

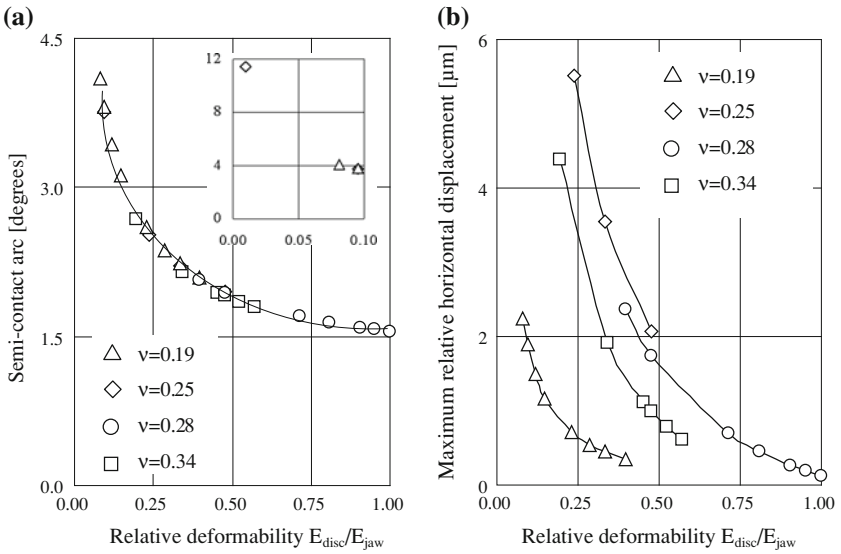

Fig. 7 Influence of relative deformability of disc and jaw materials for four different classes of Poisson's ratio. **a** Extent of the semi-contact arc. **b** Maximum relative horizontal displacement

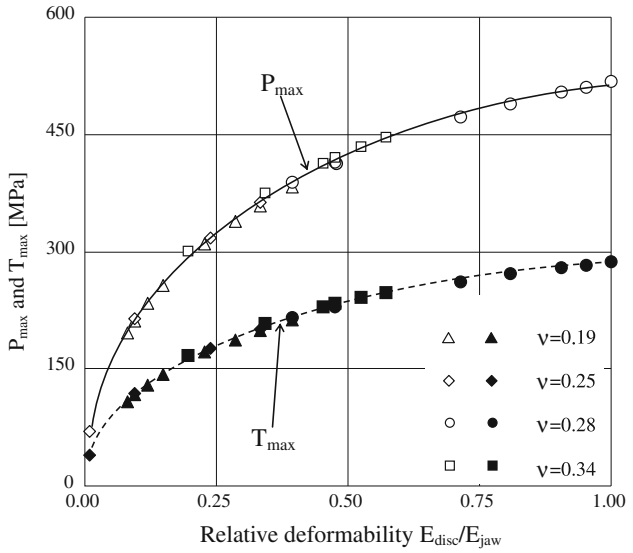

Fig. 8 Dependence of maximum radial pressure $P_{\max} = P(0)$ and maximum frictional stress $T_{\max} = T(2\ell/3)$ on relative deformability of disc and jaw materials for four different classes of Poisson's ratio

once again that despite their similarity, the curves for $P_{\max}$ and $T_{\max}$ do not represent quantities corresponding to the same τ: indeed, while $P_{\max}$ appears at $\tau = 0$, $T_{\max}$ appears constantly at $\tau = 2\ell/3$. It is also noted that as the ratio $E_{\text{disc}}/E_{\text{jaw}}$ tends to unity, the maximum values of both $P_{\max}$ and $T_{\max}$ attain extremely high values (even compared to the failure stress of the respective materials) due to the corresponding reduction in contact length.

4.2 Influence of the load level

The level of the externally applied load is expected to strongly influence all the crucial quantities related to the frictional stresses developed at the disc–jaw interface. What is perhaps not expected is that in some cases this dependence is not linear. As mentioned previously, only two cases are considered for the disc material, namely Dionysos marble ($E_1 = 80\,\text{GPa},\ \nu_1 = 0.25$) and PMMA ($E_1 = 3.2\,\text{GPa},\ \nu_1 = 0.36$). The variation

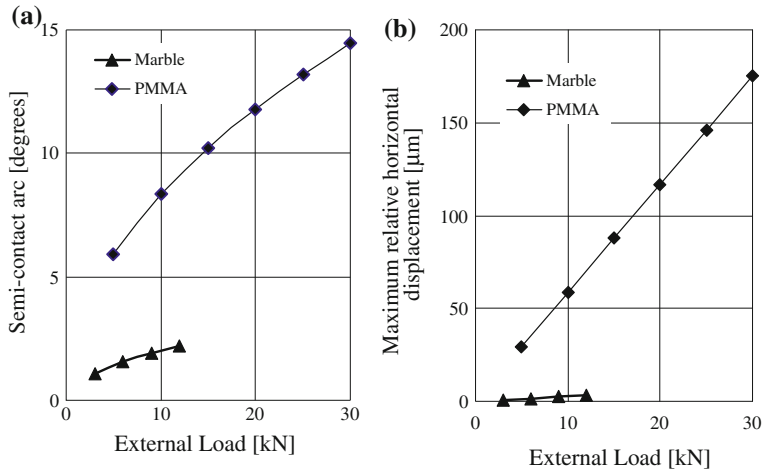

Fig. 9 Influence of externally applied load for discs of Dionysos marble and PMMA. **a** Variation of semi-contact arc. **b** Maximum relative horizontal displacement

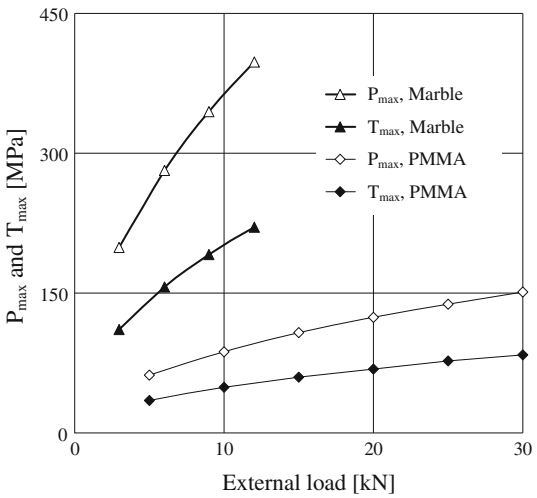

Fig. 10 Dependence of the maximum radial pressure $P_{\max} = P(0)$ and maximum frictional stress $T_{\max} = T(2\ell/3)$ on externally applied load for discs of Dionysos marble and PMMA

of the semi-contact arc for these materials versus the load applied by the loading frame on the jaw is plotted in Fig. 9a. For marble, it is seen that the contact semi-arc for a load ($P_{\text{dev}} = 12$ kN) approaching the failure load is about 2°. In contrast, for PMMA, and for a load ($P_{\text{dev}} = 30$ kN) approaching that causing yield [20], the semi-contact arc is about 15°. Higher loads are not considered since the present analysis is valid only for linear elastic materials. The results for PMMA discs were recently verified experimentally using the digital image correlation technique [21]. For marble, the corresponding test results are very difficult to obtain because the contact arc is so small, even for loads approaching the failure load.

Concerning the dependence of the maximum value of displacement mismatch on the external load, it is seen from Fig. 9b that the differences between marble and PMMA are huge. For PMMA, the maximum value is about 175 μm (for $P_{\text{dev}} = 30$ kN), while for marble, the maximum value (for $P_{\text{dev}} = 12$ kN) is about 3.5 μm (i.e. almost 50 times lower).

The maximum values of radial pressure and frictional stress versus the applied load are plotted in Fig. 10 and are much higher for marble than for PMMA. If $P_{\text{dev}} = 12$ kN, for example, the maximum radial pressure $P(0)$ for marble approaches 400 MPa, while for PMMA it is about 80 MPa. Similarly, the maximum frictional stress $T(2\ell/3)$ for marble exceeds 200 MPa, while that for PMMA is around 50 MPa. Clearly, the stress field in the immediate vicinity of the contact area is much more intense in the case of marble and might possibly

lead to premature failure, thereby undermining the validity of the test. On the other hand, the stress field for PMMA is weaker, and it appears that failure in this region is far less likely.

4.3 Role of geometry

In this section the possible influence of the size of the loading device, as represented by the radius of curvature of the jaw (and therefore by the disc radius, since $R_{\text{jaw}} = 1.5R_{\text{disc}}$, according to the ISRM-suggested device [13]), on the results of the Brazilian test is assessed. Thus, the semi-contact arc and semi-contact length are plotted in Fig. 11 versus the disc radius for a constant value of the external load (10 kN). It is noted that for both materials considered in this section (marble and PMMA), the contact arc varies according to a strongly non-linear law with respect to the disc radius, although this arc tends to stabilize for discs of radius greater than around 200 mm.

The dependence of the maximum radial pressure and of the maximum frictional stress on the disc radius, plotted in Fig. 12 for $P_{\text{dev}} = 10$ kN, is again strongly nonlinear in the 20 mm $< R_{\text{disc}} <$ 200 mm interval. For both marble and PMMA, these maximum values tend to stabilize for disc radii greater than 200 mm.

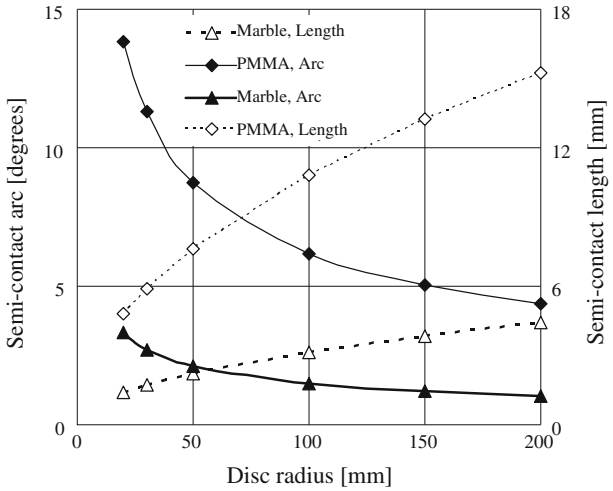

Fig. 11 Influence of disc radius on extent of semi-contact arc and semi-contact length for discs of Dionysos marble and PMMA ($P_{\text{dev}} = 10$ kN)

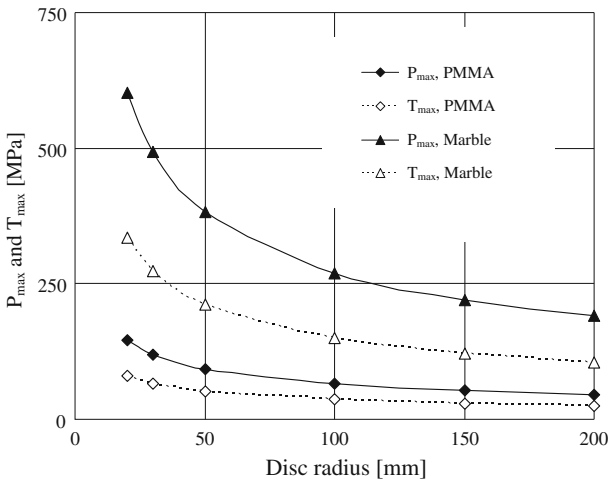

Fig. 12 Dependence of maximum radial pressure $P_{\max} = P(0)$ and maximum frictional stress $T_{\max} = T(2\ell/3)$ on disc radius for Dionysos marble and PMMA ($P_{\text{dev}} = 10$ kN)

5 Discussion and conclusions

A novel approach for determining the boundary conditions at the disc–jaw interface in the Brazilian disc test is presented, overcoming some weaknesses in existing approaches. Advantage was taken of recent studies which permitted the determination of both the length of the contact arc and the real distribution of radial pressure developed due to the compression of the jaw against the disc, contrary to current practice which assigns arbitrary values to both quantities (i.e. the contact arc is considered "very small" of the order of "some degrees", while the pressure variation is assumed to be uniform).

Emphasis is given to the interfacial friction stresses developed in cases where the contact surfaces are not perfectly smooth. According to the present approach, the underlying phenomenon responsible for generating friction stresses is the different deformability of the disc and jaw materials, which in turn is responsible for the differential lateral displacement of points on the disc and jaw initially facing each other. Therefore, if the coefficient of friction is nonzero, tangential (frictional) stresses are developed, the magnitude of which is bounded by the upper limit set by the Amontons–Coulomb law of dry friction. Hence, part of the interface is characterized by perfect sticking, and elsewhere by frictional slip.

In this context, a two-branch function is introduced for the frictional stress in the contact region. The first branch is valid as long as the force tending to cause the relative displacement of points facing each other in the contact region does not exceed the potential threshold value set by the Amontons–Coulomb law. The second branch is simply the classic Amontons–Coulomb's law for dry friction, wherein the force tending to cause relative displacement exceeds the critical threshold.

The main issue to be answered now is the accurate experimental determination of the coefficient f, which correlates the displacement mismatch and the radial pressure with the force tending to cause relative displacement at the interface. In addition, an analysis of the factors which govern the magnitude of this coefficient must be undertaken.

According to the results of the present analysis, the distributions of frictional stress along the semi-contact rim are strongly skewed without any symmetry. They are zeroed both at the axis of symmetry and at the ends of the contact arc and attain their maximum value at a distance equal to two-thirds of the semi-contact arc. Earlier studies clearly support at least qualitatively the results of the present study. In addition, it is shown that the relative deformability of the two materials (that of the disc and jaw) as represented by the ratio $E_{\text{disc}}/E_{\text{jaw}}$ is the most crucial factor, since it governs the magnitude of the displacement mismatch.

Concerning the dependence of the maximum value of the friction stress on all three quantities entering into the analysis (relative deformability, externally applied load and radius of specimen), it is demonstrated that it is of a non-linear nature.

Finally, it is indicated that the relative size of the contact arc varies between extremely broad limits for different disc materials, and therefore, assigning to it arbitrary values may lead to erroneous results. The same is true for the peak value of the radial pressure, since for stiff disc materials it attains very high values which can lead to local stress concentrations that are not predicted by the uniform pressure distribution usually adopted in theoretical analyses.

References

1. Carneiro, F.L.L.B.: A new method to determine the tensile strength of concrete. In: Proceedings of the 5th Meeting of the Brazilian Association for Technical Rules, 3rd. Section, 16 September 1943, 126–129 (in Portuguese)
2. Akazawa, T.: New test method for evaluating internal stress due to compression of concrete (the splitting tension test) (part 1). J. Jpn. Soc. Civil Eng. **29**, 777–787 (1943)
3. Fairhurst, C.: On the validity of the 'Brazilian' test for brittle materials. Int. J. Rock Mech. Min. Sci. **1**, 535–546 (1964)
4. Colback, P.S.B.: An analysis of brittle fracture initiation and propagation in the Brazilian test. In: Proceedings of 1st Congress of International Society of Rock Mechanics, pp. 385–391. Lisbon (1966)
5. Hooper, J.A.: The failure of glass cylinders in diametral compression. J. Mech. Phys. Solids **19**, 179–200 (1971)
6. Addinall, E., Hackett, P.: Tensile failure in rock-like materials. In: Spokes, E.M., Christiansen, C.R. (eds.) Proceedings of the 6th Symposium on Rock Mechanics. University of Missouri at Rolla, Rolla, pp. 515–38 (1964)
7. Lavrov, A., Vervoort, A.: Theoretical treatment of tangential loading effects on the Brazilian test stress distribution. Int. J. Rock Mech. Min. Sci. **39**, 275–283 (2002)
8. Lanaro, F., Sato, T., Stephensson, O.: Microcrack modelling of Brazilian tensile tests with the boundary element method. Int. J. Rock Mech. Min. Sci. **46**, 450–461 (2009)
9. Hudson, J.A., Brown, E.T., Rumel, F.: The controlled failure of rock discs and rings loaded in diametral compression. Int. J. Rock Mech. Min. Sci. **9**, 241–248 (1972)
10. Markides, C.F., Pazis, D.N., Kourkoulis, S.K.: The influence of friction on the stress field of the Brazilian tensile test. Rock Mech. Rock Eng. **44**, 113–119 (2011)

11. Conway, H.D., Engel, P.A.: Contact stresses in slabs due to round rough indenters. Int. J. Mech. Sci. **11**, 709–722 (1969)
12. Ghobrial, M.I.: A photoelastic investigation on the contact stresses developed in rolls during asymmetrical flat rolling. Int. J. Mech. Sci. **31**(10), 751–764 (1989)
13. ISRM (Co-ordinator: F. Ouchterlony): Suggested methods for determining the fracture toughness of rock. Int. J. Mech. Sci. Geomech. Abstr. **25**, 71–96 (1988)
14. Muskhelishvili, N.I.: Some Basic Problems of the Mathematical Theory of Elasticity. (P. Noordhoff, Groningen 1963)
15. Markides, C.F., Kourkoulis, S.K.: The stress field in a standardized Brazilian disc: The influence of the loading type acting on the actual contact length. Rock Mech. Rock Eng. **45**(2), 145–158 (2012)
16. Exadaktylos, G.E., Vardoulakis, I., Kourkoulis, S.K.: Influence of nonlinearity and double elasticity on flexure of rock beams—II. Characterization of Dionysos marble. Int. J. Solids Struct. **38**(22–23), 4119–4145 (2001)
17. Vardoulakis, I., Kourkoulis, S.K., Zambas, C.: Modeling of the mechanical behaviour of a conchyliates shellstone. In: 2nd International Symposium on Hard Soils Soft Rocks, Naples, Italy, 12–14 October 1998. Published in: Evangelista, A., Picarelli, L. (eds.) The Geotechnics of Hard Soils-Soft Rocks, pp. 911–922. A. A. Balkema, Rotterdam (1998)
18. Kourkoulis, S.K., Chatzistergos, P.E., Markides, C.F.: A combined numerical and experimental study of the displacement field in the standardized Brazilian disc test. In 10th International Congress on Mechanics, Hellenic Society for Theoretical and Applied Mechanics, Chania, Crete, Greece, 25–27 May 2013. (2013, to appear)
19. Gere, J.M.: Mechanics of Materials, 6th edn. Thomson, Toronto (2006)
20. Pazis, D.N., Agioutantis, Z., Kourkoulis, S.K.: The optical method of reflected caustics applied for a plate with a central hole: critical points and limitations. Strain **47**(6), 489–498 (2011)
21. Kourkoulis, S.K., Markides, C.F., Chatzistergos, P.E.: The Brazilian disc under parabolically varying load: theoretical and experimental study of the displacement field. Int. J. Solids Struct. **49**(7–8), 959–972 (2012)